



**HAL**  
open science

**Ultrasonic characterization and multiscale analysis for  
the evaluation of dental implant stability: a sensitivity  
study Biomedical Signal Processing and Control 42  
(2018) 37-44**

I Scala, G. Rosi, V.-H Nguyen, R Vayron, G Haiat, S Seuret, S Jaffard, S Naili

► **To cite this version:**

I Scala, G. Rosi, V.-H Nguyen, R Vayron, G Haiat, et al.. Ultrasonic characterization and multiscale analysis for the evaluation of dental implant stability: a sensitivity study Biomedical Signal Processing and Control 42 (2018) 37-44. Biomedical Signal Processing and Control, 2018, 10.1016/j.bspc.2017.12.007 . hal-01786534

**HAL Id: hal-01786534**

**<https://hal.science/hal-01786534>**

Submitted on 5 May 2018

**HAL** is a multi-disciplinary open access archive for the deposit and dissemination of scientific research documents, whether they are published or not. The documents may come from teaching and research institutions in France or abroad, or from public or private research centers.

L'archive ouverte pluridisciplinaire **HAL**, est destinée au dépôt et à la diffusion de documents scientifiques de niveau recherche, publiés ou non, émanant des établissements d'enseignement et de recherche français ou étrangers, des laboratoires publics ou privés.

# Ultrasonic characterization and multiscale analysis for the evaluation of dental implant stability: a sensitivity study

Biomedical Signal Processing and Control 42 (2018) 37-44

I. Scala<sup>a</sup>, G. Rosi<sup>a</sup>, V.-H. Nguyen<sup>a</sup>, R. Vayron<sup>a</sup>, G. Haiat<sup>a</sup>, S. Seuret<sup>b</sup>, S. Jaffard<sup>b</sup>, S. Naili<sup>a,\*</sup>

5 <sup>a</sup>Université Paris-Est, Laboratoire Modélisation et Simulation Multi Echelle, MSME UMR 8208 CNRS, 61, Avenue du Général de Gaulle, 94010 Créteil, France

<sup>b</sup>Université Paris-Est, LAMA UMR 8050, UPEM, UPEC, CNRS, 61, Avenue du Général de Gaulle, 94010 Créteil, France

---

## Abstract

With the aim of surgical success, the evaluation of dental implant long-term stability is an important task for dentists. About that, the complexity of the newly formed bone and the complex boundary conditions at the bone-implant interface induce the main difficulties. In this context, for the quantitative evaluation of primary and secondary stabilities of dental implants, ultrasound based techniques have already been proven to be effective. The microstructure, the mechanical properties and the geometry of the bone-implant system affect the ultrasonic response.

The aim of this work is to extract relevant information about primary stability from the complex ultrasonic signal obtained from a probe screwed to the implant. To do this, signal processing based on multiscale analysis has been used. The comparison between experimental and numerical results has been carried out, and a correlation has been observed between the multifractal signature and the stability. Furthermore, a sensitivity study has shown that the variation of certain parameters (*i.e.* central frequency and trabecular bone density) does not lead to a change in the response.

10 **Keywords:** implant stability; multiscale analysis; numerical simulations; sensitivity study; wave propagation

---

## 1 Introduction

A correct evaluation of dental implant stability is crucial for surgical success. First of all, two types of stability are of interest: i) primary or mechanical stability and ii) secondary or biological stability. Primary stability is reached during the implant placement, while secondary stability occurs after bone remodeling and osteo-integration. It is proven that long-term anchorage of a dental implant depends on the quantity and quality of the surrounding bone tissue,

---

\*Corresponding author

Email addresses: [ilaria.scala@u-pec.fr](mailto:ilaria.scala@u-pec.fr) (I. Scala), [giuseppe.rosi@u-pec.fr](mailto:giuseppe.rosi@u-pec.fr) (G. Rosi), [vu-hieu.nguyen@u-pec.fr](mailto:vu-hieu.nguyen@u-pec.fr) (V.-H. Nguyen), [romain.vayron@u-pec.fr](mailto:romain.vayron@u-pec.fr) (R. Vayron), [haiat@u-pec.fr](mailto:haiat@u-pec.fr) (G. Haiat), [seuret@u-pec.fr](mailto:seuret@u-pec.fr) (S. Seuret), [jaffard@u-pec.fr](mailto:jaffard@u-pec.fr) (S. Jaffard), [naili@u-pec.fr](mailto:naili@u-pec.fr) (S. Naili)

Preprint submitted to Elsevier

May 5, 2018

the peri-implant bone. Indeed, the bone remodeling occurring at the bone-implant interface [8] leads to changes in the bone mechanical properties [14]. From a mechanical point of view, modeling difficulties are mostly due to the complexity of newly formed bone tissue (a complex, anisotropic, porous-viscoelastic medium in constant remodeling), to its multiscale and time-evolving nature [7], but also to the boundary conditions at the bone-implant interphase. This means that primary and secondary stabilities are affected by several parameters, as bone quality, bone density or amount of bone in contact with the implant.

In literature, ultrasound based techniques have already been proven to be effective in the quantitative evaluation of primary and secondary stabilities of dental implant [15, 16, 18, 19, 20, 21], for both experiments and numerical simulations. The technique is based on the following assumptions: i) dental implants act as wave guides for ultrasounds; ii) propagation in wave guides is considerably affected by changes in boundary conditions, *i.e.* by different levels of stability. The objective is to inspect the ultrasonic response of the implant information and correlate it to the evolution of stability, by using signal processing techniques. As already pointed out, the ultrasonic response depends on parameters like bone structure, geometry or mechanical properties, which, *in vivo*, all vary in parallel, and whose effect on stability is not clear. Thus, with the aim of analyzing the effect of these parameters, mechanical modeling is a key resource. Indeed, numerical simulation is advantageous with respect to experiences because it can perform, in a controlled manner, a sensitivity analysis with respect to parameters such as bone density and stiffness.

Now, two main issues arise: i) how to evaluate the specific signature left from the aforementioned parameters on the signal and ii) the extraction of the information.

Therefore, the signal issued from the measurements is complex. In recent studies developed by our group, the envelope of the signal has been taken into account in signal processing (see *e.g.* [20]). In the literature, similar irregular and complex biological data have already been approached with fractal and/or multifractal analysis [4, 9, 10], with the aim of characterization and classification of complex signals. In order to analyze the signal in its wholeness, more advanced signal processing techniques based on wavelet techniques have been introduced in the context of multifractal analysis; but we will use them with a slightly different purpose since, as we will see, multifractal analysis as such cannot be performed for such signals.

Following the technique employed in [15, 16, 18, 19, 20, 21] different levels of implant stability will be artificially induced by a progressive unscrewing on the dental implant. This configuration has been used in both experimental and numerical analysis. The numerical results are obtained by using the finite element method.

This paper is structured as follows. After this introduction, Section 2.1 introduces the geometrical configuration of the problem (for which, with the aim of simplifying calculations, an axisymmetric geometry has been considered) and then provides the axial symmetric equations of motion; also the Finite Element (FE) analysis is introduced. Then, Section 3 presents a rapid overview on the wavelet based multiscale analysis. Section 4 is devoted to the presentation and discussion of the obtained results. Finally, Section 5 sets out conclusion and some perspectives.

## 2 Modeling wave propagation in the bone-implant system

### 2.1 Geometrical configuration and governing equations

The geometrical configuration reported in Fig. 1 shows the axial symmetry with respect to the implant central axis. According to that, an axisymmetric 2D model has been used. A contact

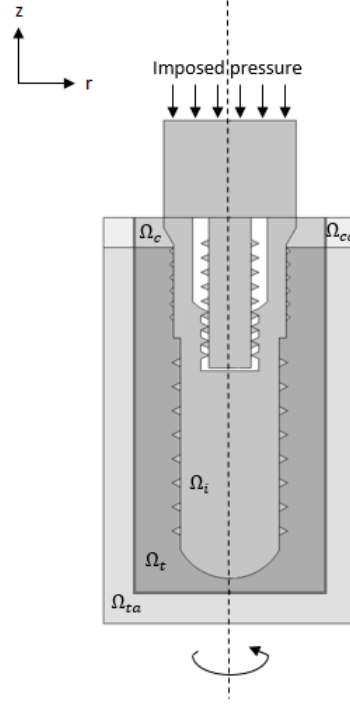


Figure 1: Cross-section view of the 3-D axisymmetric geometrical configuration used in the numerical simulations. The domains are denoted with a subscript corresponding to the trabecular bone ( $\Omega_t$ ), the cortical bone ( $\Omega_c$ ), the implant ( $\Omega_i$ ), and the absorbing layers associated to trabecular and cortical bone ( $\Omega_{ta}$  and  $\Omega_{ca}$ , respectively).

planar transducer is placed on the emerging surface of the implant. A double-layer structure of a cortical bone 1 mm thick and an half-space of trabecular bone compose the considered bone model. In the geometrical configuration shown in Fig. 1, the titanium dental implant commercialized by Implants Diffusion International (IDI1240, IDI, Montreuil, France), with a length of  $L = 11.5$  mm and a diameter of  $D = 4$  mm, is recreated. In addition, a specific healing abutment is inserted in the upper part of the implant. When the implant is totally inserted in the bone specimen, as it is in the configuration considered in this work, we deal with the typical clinical set-up. In the present study, volume forces are neglected and it is assumed that all the considered media exhibit isotropic homogeneous mechanical properties. The cylindrical coordinates are used and designated by  $(r, \theta, z)$ .

The axisymmetric equations of motion in each subdomain are the following:

$$\rho \ddot{u}_r - \frac{\partial \sigma_{rr}}{\partial r} - \frac{1}{r} \frac{\partial \sigma_{rz}}{\partial z} - \frac{\sigma_{rr} - \sigma_{\theta\theta}}{r} = 0, \quad (1)$$

$$\rho \ddot{u}_z - \frac{\partial \sigma_{zz}}{\partial z} - \frac{\sigma_{rz}}{r} = 0, \quad (2)$$

where  $\rho$  stands for the mass density,  $u_r$  and  $u_z$  represent, respectively, the radial and axial components of the displacement vector;  $\sigma_{rr}$ ,  $\sigma_{rz}$ ,  $\sigma_{\theta\theta}$ ,  $\sigma_{zz}$  are the components of the stress tensor  $\sigma$ ; furthermore, the double dot indicates the temporal second partial derivative. According to Hooke's relation, the constitutive relation for an isotropic homogeneous material can be expressed as:

$$\sigma = \frac{E\nu}{(1+\nu)(1-2\nu)} \text{Tr}(\epsilon)\mathbb{I} + \frac{E}{1+\nu} \epsilon \quad (3)$$

80 where  $E$  and  $\nu$  are Young's modulus and Poisson coefficient, respectively,  $\text{Tr}()$  is the trace operator of a tensor,  $\mathbb{I}$  is the identity tensor and  $\epsilon$  is the strain tensor whose non-zero components are given by:

$$\epsilon_{rr} = \frac{\partial u_r}{\partial r}, \quad \epsilon_{\theta\theta} = \frac{u_r}{r}, \quad \epsilon_{rz} = \frac{1}{2} \left( \frac{\partial u_r}{\partial z} + \frac{\partial u_z}{\partial r} \right), \quad \epsilon_{zz} = \frac{\partial u_z}{\partial z}. \quad (4)$$

Young's modulus has been considered to be related to the density  $\rho$  according to the following power-law relation [5]:

$$E = E_0 \left( \frac{\rho}{\rho_0} \right)^{1.96}, \quad (5)$$

85 where the subscript  $_0$  indicates the reference values for the Young's modulus and the density.

The contact planar transducer, placed on the upper emerging surface of the implant specimen (see Fig. 1), generates a signal corresponding to a time pulse uniform pressure whose temporal history is expressed as follows:

$$p(t) = A \left[ \exp -4(f_c t - 1)^2 \right] \times \sin(2\pi f_c t), \quad (6)$$

where  $A$  is the amplitude,  $f_c$  is the pulse central frequency and  $t$  is the time.

90 The continuity of displacement and stress fields between the subdomains is imposed. Moreover, in order to prevent the nonphysical reflected wave generated from the lateral and bottom boundaries of the bone domains, an absorbing layer has been added to the model, as shown in Fig. 1.

The domain is at rest for  $t < 0$ , *i.e.* stress and displacement are set to zero everywhere in the domain. At  $t = 0$ , the uniform pressure given by Eq. (6) is imposed on the upper emerging surface of the implant specimen.

## 2.2 Finite element simulation

In this subsection, the resolution method is described. The boundary value problem defined in subsection 2.1 was solved by using the software COMSOL Multiphysics (Stockholm, Sweden) 100 which is based on the finite element method.

By the discretization of the equations, a linear system of ordinary differential equations is obtained, which is solved by an implicit generalized  $\alpha$ -method in the time domain, a complete description of which can be found in [20]. Briefly, an unstructured mesh of triangular finite elements with quadratic Lagrange interpolating polynomials was used. A critical choice 105 for the convergence of the numerical results concerns the steps of the temporal and spatial discretization. Thus, the element's size of each subdomain (see Fig. 1) was chosen equal to  $\lambda_{min}/10$ , where  $\lambda_{min}$  represents the smallest wavelength in the domain and it can be computed as  $\lambda_{min} = c_{min}/f_{max}$  (for the isotropic elastic media considered here,  $c_{min}$  is the shear wave velocity) and  $f_{max}$  the maximum value of the frequency range. For this reason, we considered 110 meshes with smoothly varied sizes of elements when there are interfaces between two materials. The mesh of the considered model contains around  $10^6$  degrees of freedom. The time step has been chosen in order to respect the Courant-Friedrichs-Lewy (CFL) condition, which represents a necessary condition for stability. Thus, in these simulations, the time step is set equal to  $1.5 \times 10^{-9}$  s.

## 115 2.3 Indicator of the implant stability

The ultrasonic response of the implant is measured by using an echographic mode. The output radio frequency (rf) signal was determined by computing the spatial average of the pressure at the upper surface of the implant (see Fig. 1). In order to extract information, in [18, 19], the signal envelope, that is the smooth curve outlining the extremes of the signal, has been  
120 considered to build an indicator as a scalar quantity proportional to the implant stability. This indicator is indeed based on the temporal variation of the signal amplitude and is defined as:

$$I = \sum_{i=1}^N S(it_0) \quad (7)$$

where  $N$  designates the samples number,  $t_0$  is the sampling rate and  $S(t)$  the signal envelope. As an example, in Fig. 2, an output signal obtained with our ultrasonic device is presented.

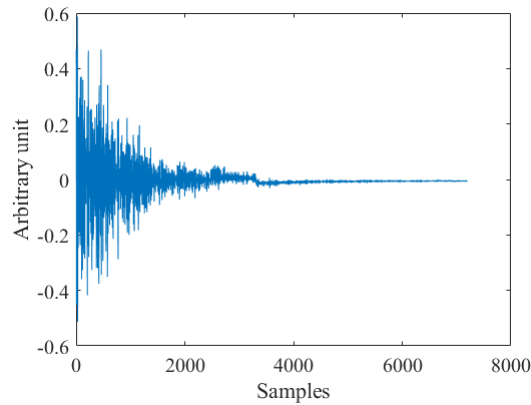


Figure 2: Example of an output signal obtained with our ultrasonic device.

In this work we want to extend the signal processing analysis to the inner structure of the  
125 signal. Indeed, since the recorded signal came from multiple reflections at the interface bone-implant, a multi-scale or multi-fractal analysis seems to be appropriate. Details about this signal processing technique will be given in the next section.

## 3 Signal processing and multiscale analysis

Multifractal analysis has been already employed in medicine to discriminate bone pathologies  
130 like osteoporosis [9, 12], to characterize microstructure of porous media (and, in particular, bone tissue) [17] and infectious diseases [11], to differentiate dentate and edentulous regions [24] and more.

In this work, multifractal tools are employed to extract relevant information from the scaling properties of signals either derived from experimental and numerical data. The aim  
135 is to discriminate the implant stability. Multifractal analysis consists in determining *structure functions* associated with the data and discussing their relevance using classification methods or model selection.

### 3.1 Wavelet basis

Starting with the scaling function  $\phi(x)$  and the wavelet  $\psi(x)$  (regular and well localized), an  
140 orthonormal wavelet basis on  $L^2(\mathbb{R})$  (where  $L^p(\mathbb{R})$  is the Lebesgue space of  $p$ -power integrable

functions on real numbers  $\mathbb{R}$ ) is defined as the set of functions  $\phi(x - k)$  and  $2^{j/2}\psi(2^j x - k)$ , where natural number  $j \geq 0$  and  $k \in \mathbb{Z}$  for which  $j$  and  $k$  are natural numbers belonging to  $\mathbb{Z}$ . The basis is " $r$ -smooth" if  $\phi(x)$  and  $\psi(x)$  have derivatives up to order  $r$  which have fast decay. The quantity  $r$  is a parameter which has to be picked larger enough depending on the data analyzed; indeed it has to be larger than the highest Hölder exponent present in the data. We denote by  $c_{j,k}$  and  $c_k$  the *wavelets coefficients* on the function  $f$ , which are defined by:

$$c_{j,k} = 2^j \int_{\mathbb{R}} f(x)\psi(2^j x - k)dx, \quad c_k = \int_{\mathbb{R}} f(x)\phi(x - k)dx. \quad (8)$$

These coefficients give information on the oscillations of  $f$  in the neighborhood of the dyadic interval  $\lambda(= \lambda(j, k)) := [k2^{-j}, (k + 1)2^{-j})$ , which leads to a more compact notation, that is  $c_\lambda = c_{j,k}$  and  $\psi_\lambda(x) = \psi(2^j x - k)$ . This kind of indexation is useful because the wavelet  $\psi_\lambda$  is fundamentally located near the dyadic interval  $\lambda$ . Furthermore, we denote by  $\Lambda_j$  the set of dyadic intervals  $\lambda$  of width  $2^{-j}$ . A  $L^1(\mathbb{R})$  normalization for wavelet coefficients is used because it is more natural in order to express scale invariance relations.

### 3.2 Wavelets structure functions

The wavelet structure functions of  $f$  are defined by:

$$\forall j \in \mathbb{N}, \quad \forall p > 0, \quad S_f(p, j) = 2^{-j} \sum_{\lambda \in \Lambda_j} |c_\lambda|^p, \quad (9)$$

where  $\mathbb{N}$  refers to the set of all natural numbers.

Multifractal analysis usually proposes to use classification tools based on log-log plot regressions of structure functions (the so-called *scaling functions*, see [1, 2]). However, in our case, log-log plots do not display a clear scaling-invariance behavior (see Figure 3). Therefore, it seems more relevant to base classification directly on the structure functions (note that a similar idea was followed in [3] for old photographic papers). One possibility is to consider quantities which are used in the wavelet characterization of homogeneous Besov spaces  $\dot{B}_p^{0,p}(\mathbb{R})$  (the space  $\dot{B}_p^{0,p}(\mathbb{R})$  is closely related with the  $L^p(\mathbb{R})$  space, see [1, 2]). Besov regularity and the explicit estimation of Besov norms are widely used in signal and image processing, since equivalent norms were derived by Y. Meyer and D. Donoho and his collaborators who showed how they can be used in denoising algorithms and inverse problems, see *e.g.* [6]. Recall that the wavelet characterization of these spaces implies that, if wavelets are smooth enough (which we assume), then

$$\| f \|_{\dot{B}_p^{0,p}(\mathbb{R})}^p \sim \sum_j 2^{-j} \sum_{\lambda \in \Lambda_j} |c_\lambda|^p = \sum_j S_f(p, j). \quad (10)$$

## 4 Results and discussion

To realize this study, we used the Wavelet Leader and Bootstrap [22, 23] based multifractal analysis (WLBMF) toolbox. This analysis has been performed to both experimental data and numerical simulations. As stated above, the signals we deal with have, from a qualitative point of view, a complex structure, thus the aim is to extract a quantification of implant stability, and study the sensitivity of this method with respect to changes in bone density, stiffness and with respect to the probe central frequency.

In both experiments and simulations, the variation of stability has been induced in a controlled

manner by a progressive unscrewing of  $2\pi$ -rad of the dental implant, that, in what follows, will be indicated by the number of rotations  $R$ . Higher values of the rotation parameters correspond to lower stabilities.

## 4.1 Structure functions

180 The consideration of structure functions for classification purposes goes back to the seminal work of Kolmogorov in turbulence in 1941 [13], and their wavelet counterpart was introduced by A. Arneodo and his collaborators at the end of the 1980's.

The results presented in what follows correspond to a specific selection of process parameters settings for the WLBMF toolbox. The two standard analysis methods have been performed, 185 *i.e.* the discrete wavelet transform coefficients (DWT) and the Leaders' wavelets (LWT), with  $N_\psi = 3$  vanishing moments. The choice of a wavelet basis requires:

- (i) the shortness of the filters (which implies faster decomposition algorithms and a larger number of scales on which log-log plot regressions can be computed for the determination of scaling exponents);
- 190 (ii) the regularity of the wavelets and the number of vanishing moments (which allow to deal with larger classes of signals displaying a wider range of singularity exponents).

These two requirements are contradictory, since, for a given class of wavelets, the longer the filters the more vanishing moments. However, when no specific additional requirement is needed (such as *e.g.* a symmetry for the filters) Daubechies wavelets present an optimal 195 compromise, and therefore are usually preferred. So, in what follows, the results presented derive from using Daubechies wavelets.

The scaling range was chosen as  $3 \leq j \leq 7$ . Over these scales a weighted polynomial regression has been performed. Moreover, we remarked that information can be extracted only for  $p \in [1, 3]$ , and that the information is equivalent for each  $p$  in this range. Thus, in 200 what follows, we assume that  $p = 1$ .

As stated above, this analysis is performed on experimental and numerical data. For the experiments, with the aim of reproducing the buccal condition, the configuration considered presents a bone porous structure saturated with water and completely immersed. All simulations have been performed by means of the commercial software COMSOL Multiphysics (Stockholm, 205 Sweden).

We start the analysis by the computation of the structure functions (which examine power-law relations for all orders of moments) related to experimental tests and a numerical simulation, in order to extract their main features. The results are plotted in Fig. 3, for different levels of stability. From the analysis of the structure functions, and their evolution with respect to 210 rotations, the following observations may be exposed:

- small scales (*e.g.*  $j < 3$ ) do not include any information, in fact they are invariant for each case considered;
- large scales (*e.g.*  $j > 6$ ) correspond to phenomena not taken into account, such as large fluctuations due to measurement conditions (*e.g.* small movements of the probe);
- 215 – following the previous considerations, it is reasonable to take into account only the scale corresponding to  $j \in [3, 6]$  ;

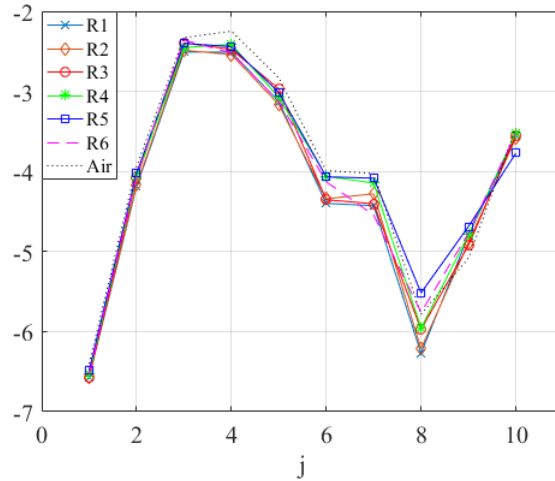


Figure 3: (Colors online). Wavelet structure functions (DWT) (for  $p = 1$ ) performed on the experimental data. On the top right corner a legend for the curves is presented, where "R1" represents the implant fully inserted in bone tissue, "R*i*" ( $i = 1, \dots, n$ ) the implant unscrewed of  $2 \times i\pi$ -rad, and "Air" the implant located in the air (which means that there is not bone tissue around the implant).

- in contradistinction with what is usually met in signal processing, deriving scaling exponents from log-log plots based on such data would not be relevant here.

Using such exponents for classification is the starting point of multifractal analysis methods. Since this is not appropriate here, we will rather base the classification on the richer information supplied by the collection of structure functions at different scales. Note that this option has already shown to be relevant in a different context: for ancient photographic papers classification, structure functions are not scaling invariant because of the typical scales due to the texture of the paper, and classification is performed on structure functions (see [3]).

In the region of interest (ROI) we can observe that: i) the structure functions do not exhibit a linear behaviour; ii) the shape does not seem to depend on the configuration. In this context, log-log regressions are not meaningful. As already mentioned earlier in this section, this is not uncommon in multiscale analysis, as structure functions are used also for classification with respect to their shape or the mean values. In light of these observations, mean values have been used in this work.

With the aim of validating this new technique with respect to the results presented in [18, 19, 20, 21], the same simulation with trabecular bone density  $\rho = 1170 \text{ kg/m}^3$  and central frequency  $f_c = 10 \text{ MHz}$  are compared for the indicator  $I$ , computed following Eq. (7), and the mean value of the structure functions.

Therefore, following the classification method described in section 3.2, a polynomial regression on the mean values of the structure functions (see Fig. 4b) with respect to the unscrewing has been performed. Figure 4b illustrates the results for the mean values of the structure functions and, by a comparison with Fig. 4a, the coherence with the results for both methods can be appreciated. These results show that a correlation can be clearly observed. A polynomial regression, where the fitted equation presents a quadratic form, well describes the trend of the presented results.

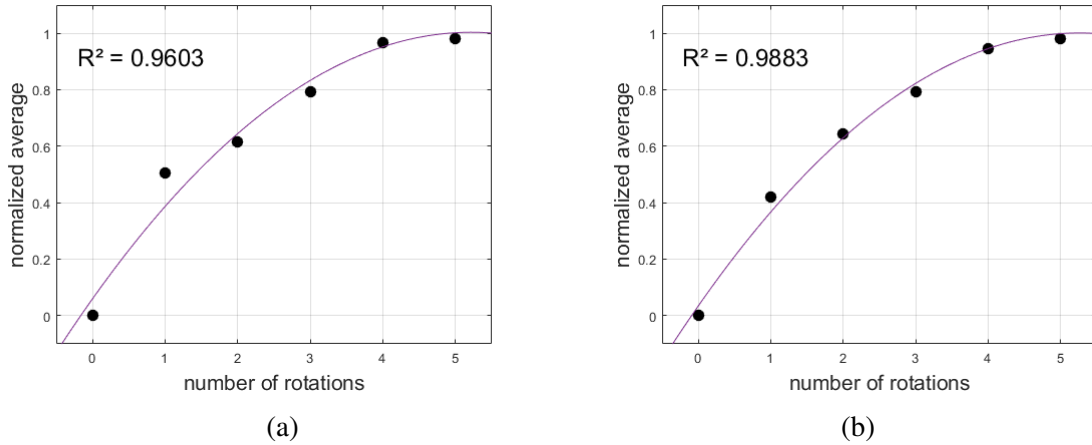


Figure 4: (Colors online). Polynomial regression for a) the indicator  $I$  and b) the mean values of the structure functions (for  $p = 1$ ).

The fact that the mean value of the structure functions increases when the stability is reduced is consistent with the mechanical interpretation of the phenomenon. Indeed, the higher the stability, the more easily the mechanical energy can flow to the surrounding tissues. When the stability is decreased, only a fraction of energy can leave the implant, leading to an higher amplitude of the ultrasonic field. In the specific case considered here, with each rotation of the implant the contact surface with bone is reduced, and so is the mechanical energy flowing out. In addition, the R-squared coefficient is indicated in the upper left of each figures. This coefficient results to be very close for both cases under exam (see Figs. 4a and 4b). Additionally, Figs. 4a and 4b underline a saturation for low level of stability (*i.e.* for increasing number of rotations).

## 4.2 Sensitivity study

A sensitivity study has been performed in order to test if parameters as trabecular bone density  $\rho$  and excitation frequency  $f_c$  have an influence on the multiscale study. Actually, the aim of a sensitivity study is to observe how much the variation of the parameters influences the response.

In particular, for each implant unscrewing level, all combinations for the following parameters have been examined:

- $\rho$ : 936, 1053, and 1170 kg/m<sup>3</sup>;
- $f_c$ : 8, 9, 10, 11, and 12 MHz.

As a reminder, concerning the experiences, the reference values of the trabecular bone density and Young's modulus are given by  $\rho_0 = 1170$  kg/m<sup>3</sup> and  $E_0 = 2.2108$  GPa. In this sensitivity study, a decreasing of 20% for the trabecular bone density has been considered which carries out  $\rho = 936$  kg/m<sup>3</sup>. The variation of density and, consequently, the ones of Young's modulus are derived from Eq. (5). Moreover, it is important to point out that for all simulations the Poisson's ratio  $\nu = 0.3$  remains unchanged. Three trabecular bone densities are examined which are associated to three Young's modulus given in Tab. 1.

In this paragraph, the following "situations" will be presented and discussed:

$\rho$ (kg/m <sup>3</sup> )	$E$ (GPa)
1170	2.2108
936	1.4276
1053	1.7983

Table 1: Three trabecular bone densities associated to three Young's modulus for the sensitivity study.

- 270 – mean values of the structure functions at fixed  $p$ -value, by varying the central frequency  $f_c$  to the trabecular bone density  $\rho$ ;
- mean values of the structure functions at fixed  $p$ -value, by varying the trabecular bone density  $\rho$  to the central frequency  $f_c$ .

275 The data are presented with respect the number of rotations where the configuration associated is denoted by  $R_i$ , for  $i = 0, \dots, n$ . As already said, the configuration associated with R1 corresponds to the implant totally inserted, and then a progressive unscrewing of  $i\pi$ -rad is realized.

280 So, the mean values of the structure functions have been analyzed with respect to the variation of frequency (at a fixed value of trabecular bone density) and also to the density (at a fixed value of frequency). Figures 5a-5c show, by fixing the value of  $\rho$ , the evolution of the mean values of the structure functions to changing the frequencies. For a given frequency, the data seem to evolve with implant unscrewing. Furthermore, it is evident that the variation of  $f_c$  induces a shift of the curves, but not a distortion in their shape. Actually, starting from 8 MHz, the next curves are like shifted downwards one after another.

285 Similarly, Figs. 6a-6c show the behaviour of the mean values of the structure functions with respect to changing trabecular bone density and at fixed central frequency. Since the curves are practically superposed, no relevant information can be extracted. It can be only highlighted that a greater solicitation is observable on the implant unscrewing level R2, which corresponds to unscrew the bone implant of  $\pi$ -rad. This consideration has been confirmed also by further  
290 simulations considering lower and higher values of trabecular bone density.

Finally, to sum up, with the aim of investigating if central frequency and trabecular bone density represent incident parameters, a sensitivity study has been performed. Hence, the mean values of the structure functions have been considered with respect to the number of rotations  $R$  (*i.e.* a progressive unscrewing of the dental implant) by fixing once the central  
295 frequency, and then the trabecular bone density. The results obtained show that the response is not affected by the parameters considered.

## 5 Conclusion

300 The present work aims at providing a first evidence on the possibility to explore and exploit the multiscale structure of the ultrasonic signal for evaluating dental implant stability. In the example provided, the ultrasonic signal is obtained from a probe fixed to the implant, and the stability is artificially reduced by performing a progressive unscrewing of the implant itself.

Experimental and numerical results have been compared and then analyzed by signal processing with multiscale methods. Since the use of multifractal analysis has highlighted an absence of log-log regression, the mean values of the structure functions have been

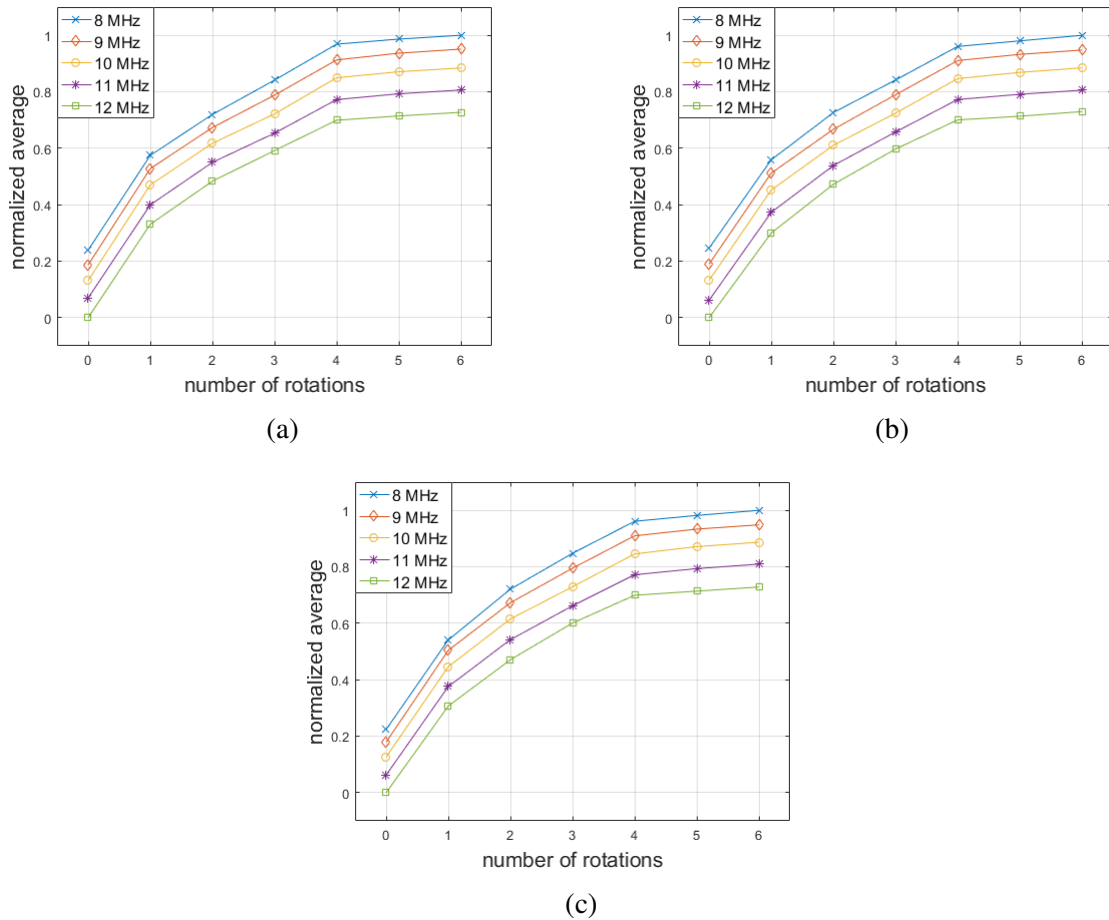


Figure 5: (Colors online). Plots of the mean values of the structure functions to the number of rotations in function of the trabecular bone density: a)  $\rho = 936 \text{ kg/m}^3$ , b)  $\rho = 1053 \text{ kg/m}^3$  and c)  $\rho = 1170 \text{ kg/m}^3$ . On the top right corner of each figure the legend is given: the different curves represent the correspondent value of central frequency.

305 considered. By comparison with the indicator used in [15, 16, 18, 19, 20, 21], a coherence between the results can be appreciated. Furthermore, a sensitivity study has been performed by varying the density of the trabecular bone and the central frequency, showing that these parameters do not have a significant incidence on the evaluation of the stability. To summarize:

- 310
- a 3D axisymmetric configuration has been used for the finite element analysis;
  - some preliminary results from multifractal analysis have been carried out;
  - the sensitivity study performed has not shown a particular incidence of the parameters investigated in this analysis.

315 With the aim of introducing a certain fractality in the mechanical model, future works may envisage the introduction of this feature from a geometrical point of view (*e.g.* by using geometrical configurations like Menger sponges and Koch iterations) as well as to find a model which contains "multifractal elements" [1, 2, 3] by using tools as the scaling exponent, the multifractal spectrum [9] or the log-cumulants.

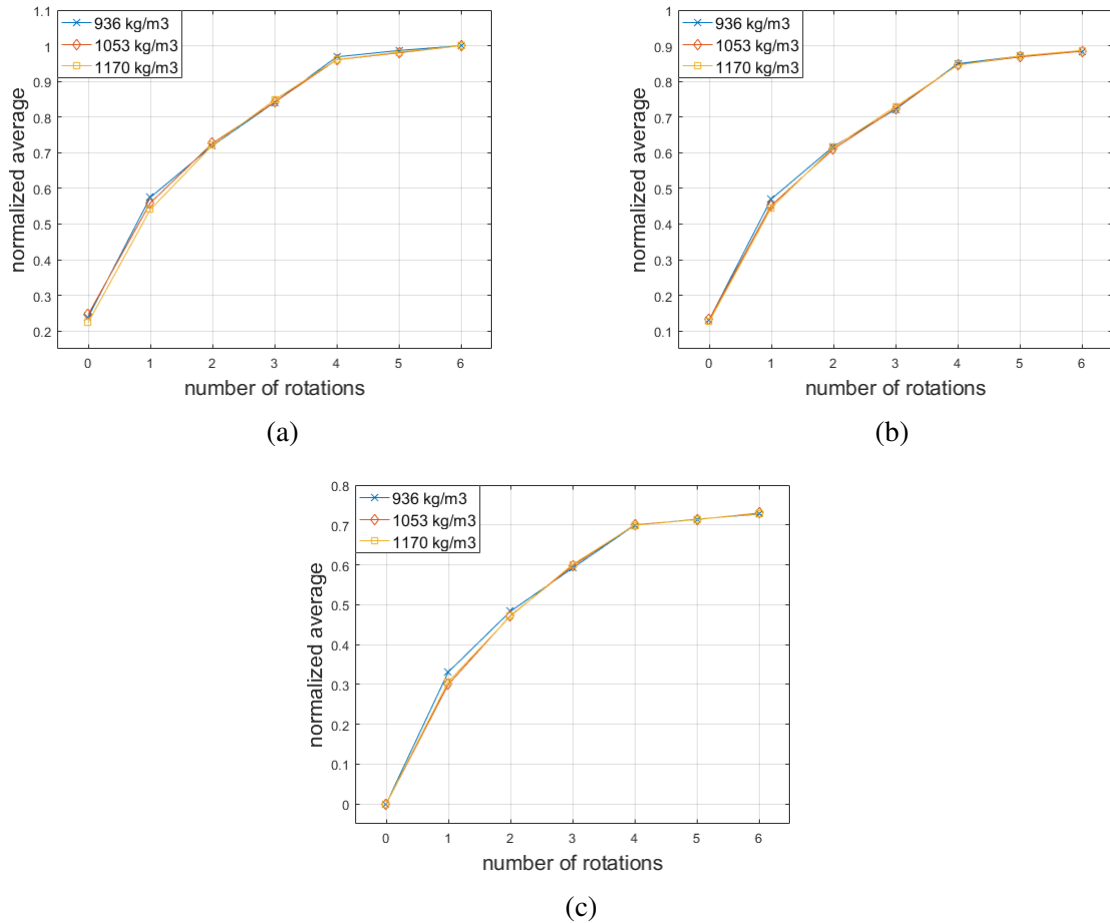


Figure 6: (Colors online). Plots of the mean values of the structure functions to the number of rotations in function of the central frequency: a)  $f_c = 8$  MHz, b)  $f_c = 10$  MHz and c)  $f_c = 12$  MHz. On the top right corner of each figure the legend is given: the different curves represent the correspondent value of trabecular bone density.

## Acknowledgments

320 This project was supported by the Université Paris-Est through the PEPS program (15R03051A-METCARMAT). This work has received funding from the European Research Council (ERC) under the European Union's Horizon 2020 research and innovation program (grant agreement No 682001, project ERC Consolidator Grant 2015 BoneImplant).

## References

- 325 [1] P. Abry, S. Jaffard, and H. Wendt. Irregularities and scaling in signal and image processing: multifractal analysis. *Benoit Mandelbrot: A Life in Many Dimensions*, pages 31–116, 2011.
- [2] P. Abry, S. Jaffard, and H. Wendt. A bridge between geometric measure theory and signal processing: Multifractal analysis. In *Operator-Related Function Theory and Time-Frequency Analysis*, pages 1–56. Springer, 2015.
- 330 [3] P. Abry, S. G. Roux, H. Wendt, P. Messier, A. G. Klein, N. Tremblay, P. Borgnat, S. Jaffard, B. Vedel, J. Coddington, et al. Multiscale anisotropic texture analysis and classification of photographic prints: Art scholarship meets image processing algorithms. *IEEE Signal Processing Magazine*, 32(4):18–27, 2015.
- [4] D. Chappard, M.-F. Baslé, E. Legrand, and M. Audran. Trabecular bone microarchitecture: a review. *Morphologie*, 92(299):162–170, 2008.
- 335 [5] S. C. Cowin, editor. *Bone mechanics handbook*. CRC Press, Boca Raton, FL, USA, 2001.

- [6] D. L. Donoho and I. M. Johnstone. Minimax estimation via wavelet shrinkage. *Ann. Statist.*, 26(3):879–921, 06 1998.
- [7] H. M. Frost. Bone’s mechanostat: a 2003 update. *The Anatomical Record Part A: Discoveries in Molecular, Cellular, and Evolutionary Biology*, 275(2):1081–1101, 2003.
- 340 [8] Y. Gabet, D. Kohavi, R. Voide, T. L. Mueller, R. Müller, and I. Bab. Endosseous implant anchorage is critically dependent on mechanostructural determinants of peri-implant bone trabeculae. *Journal of Bone and Mineral Research*, 25(3):575–583, 2010.
- [9] Z. Gao, W. Hong, Y. Xu, T. Zhang, Z. Song, and J. Liu. Osteoporosis diagnosis based on the multifractal spectrum features of micro-ct images and c4.5 decision tree. In *Pervasive Computing Signal Processing and Applications (PCSPA), 2010 First International Conference on Pervasive Computing, Signal Processing and Applications*, pages 1043–1047. IEEE, 2010.
- 345 [10] W. Geraets and P. Van der Stelt. Fractal properties of bone. *Dentomaxillofacial Radiology*, 29(3):144–153, 2000.
- [11] A. M. Holdsworth, N. K.-R. Kevlahan, and D. J. Earn. Multifractal signatures of infectious diseases. *Journal of The Royal Society Interface*, 9(74):2167–2180, 2012.
- 350 [12] M. Khider, B. Haddad, and A. T. Ahmed. Multifractal analysis by the large deviation spectrum to detect osteoporosis. In *2013 8th International Workshop on Systems, Signal Processing and their Applications (WoSSPA)*, pages 112–115. IEEE, 2013.
- [13] A. N. Kolmogorov. The local structure of turbulence in incompressible viscous fluid for very large reynolds numbers. *Proceedings: Mathematical and Physical Sciences*, 434(1890):9–13, 1991.
- 355 [14] G. Luo, A. M. Sadegh, H. Alexander, W. Jaffe, D. Scott, and S. C. Cowin. The effect of surface roughness on the stress adaptation of trabecular architecture around a cylindrical implant. *Journal of Biomechanics*, 32(3):275–284, 1999.
- [15] V. Mathieu, F. Anagnostou, E. Soffer, and G. Haiat. Numerical simulation of ultrasonic wave propagation for the evaluation of dental implant biomechanical stability. *The Journal of the Acoustical Society of America*, 129(6):4062–4072, 2011.
- 360 [16] V. Mathieu, F. Anagnostou, E. Soffer, and G. Haiat. Ultrasonic evaluation of dental implant biomechanical stability: an in vitro study. *Ultrasound in Medicine & Biology*, 37(2):262–270, 2011.
- [17] D. Sanchez-Molina, J. Velazquez-Ameijide, V. Quintana, C. Arregui-Dalmases, J. R. Crandall, D. Subit, and J. R. Kerrigan. Fractal dimension and mechanical properties of human cortical bone. *Medical Engineering & Physics*, 35(5):576–582, 2013.
- 365 [18] R. Vayron, P. Karasinski, V. Mathieu, A. Michel, D. Lorient, G. Richard, G. Lambert, and G. Haiat. Variation of the ultrasonic response of a dental implant embedded in tricalcium silicate-based cement under cyclic loading. *Journal of Biomechanics*, 46(6):1162–1168, 2013.
- [19] R. Vayron, V. Mathieu, A. Michel, and G. Haiat. Assessment of in vitro dental implant primary stability using an ultrasonic method. *Ultrasound in Medicine & Biology*, 40(12):2885–2894, 2014.
- 370 [20] R. Vayron, V.-H. Nguyen, R. Bosc, S. Naili, and G. Haiat. Finite element simulation of ultrasonic wave propagation in a dental implant for biomechanical stability assessment. *Biomechanics and Modeling in Mechanobiology*, 14(5):1021–1032, 2015.
- [21] R. Vayron, V.-H. Nguyen, R. Bosc, S. Naili, and G. Haiat. Assessment of the biomechanical stability of a dental implant with quantitative ultrasound: A three-dimensional finite element study. *The Journal of the Acoustical Society of America*, 139(2):773–780, 2016.
- 375 [22] H. Wendt, P. Abry, and S. Jaffard. Bootstrap for empirical multifractal analysis. *IEEE Signal Processing Magazine*, 24(4):38–48, 2007.
- [23] H. Wendt, S. G. Roux, S. Jaffard, and P. Abry. Wavelet leaders and bootstrap for multifractal analysis of images. *Signal Processing*, 89(6):1100–1114, 2009.
- 380 [24] F. Yaşar and F. Akgünlü. Fractal dimension and lacunarity analysis of dental radiographs. *Dentomaxillofacial Radiology*, 2014.

## Highlights

- A mechanical modeling to extract information about primary stability of an implant
- A complex ultrasonic signal obtained from a probe screwed to the implant
- Multifractal analysis has evidenced a signature of the stability
- A correlation has been observed between the multifractal signature and the stability